Block of $Ca_V1.2$ Channels by Gd^{3+} Reveals Preopening Transitions in the Selectivity Filter

Olga Babich, John Reeves, and Roman Shirokov

Department of Pharmacology and Physiology, University of Medicine and Dentistry of New Jersey, New Jersey Medical School, Newark, NJ 07103

Using the lanthanide gadolinium (Gd^{3+}) as a Ca^{2+} replacing probe, we investigated the voltage dependence of pore blockage of $Ca_V1.2$ channels. Gd^{+3} reduces peak currents (tonic block) and accelerates decay of ionic current during depolarization (use-dependent block). Because diffusion of Gd^{3+} at concentrations used (<1 μM) is much slower than activation of the channel, the tonic effect is likely to be due to the blockage that occurred in closed channels before depolarization. We found that the dose–response curves for the two blocking effects of Gd^{3+} shifted in parallel for Ba^{2+}, Sr^{2+}, and Ca^{2+} currents through the wild-type channel, and for Ca^{2+} currents through the selectivity filter mutation EEQE that lowers the blocking potency of Gd^{3+}. The correlation indicates that Gd^{3+} binding to the same site causes both tonic and use-dependent blocking effects. The apparent on-rate for the tonic block increases with the prepulse voltage in the range −60 to −45 mV, where significant gating current but no ionic current occurs. When plotted together against voltage, the on-rates of tonic block (−100 to −45 mV) and of use-dependent block (−40 to 40 mV) fall on a single sigmoid that parallels the voltage dependence of the gating charge. The on-rate of tonic block by Gd^{3+} decreases with concentration of Ba^{2+}, indicating that the apparent affinity of the site to permeant ions is about 1 mM in closed channels. Therefore, we propose that at submicromolar concentrations, Gd^{3+} binds at the entry to the selectivity locus and that the affinity of the site for permeant ions decreases during preopening transitions of the channel.

The Journal of General Physiology

INTRODUCTION

The selectivity mechanism of Ca^{2+} channels is fundamentally different from that in K^+ channels (for review see Sather and McCleskey, 2003). At submicromolar concentrations, the selectivity filter tightly binds Ca^{2+} ions that block Na^+ flux, but at higher concentrations, it permits large Ca^{2+} flux. Several theories have been put forth to reconcile the high affinity and high throughput. In one scenario, electrostatic repulsion between two Ca^{2+} ions overcomes tight binding to the selectivity filter and allows one ion to exit quickly (Almers and McCleskey, 1984; Hess and Tsien, 1984; Yang et al., 1993; Ellinor et al., 1995). This theory explains the decrease of the channel's affinity to Ca^{2+} when $[Ca^{2+}]$ is increased, as well as the markedly different apparent affinities for block of Na^+, Ba^{2+}, and Ca^{2+} conductance by polyvalent metal ions. On the other hand, both experimental data (Kuo and Hess, 1993a,b; Bahinski et al., 1997) and theoretical considerations (Armstrong and Neyton, 1991; Mironov, 1992) oppose the existence of multiple high-affinity sites and ion–ion interactions in the selectivity filter.

A second theory, proposed by Dang and McCleskey (1998), posited that two flanking low affinity Ca^{2+} sites provide energy step down to and out of the site that strongly interacts with Ca^{2+}. Despite its attractive minimalism, the stair step model cannot explain why the apparent affinity of the selectivity filter to blocking polyvalent cations strongly depends on the ion species carrying the current (e.g., Ba^{2+} vs. Ca^{2+}).

The "electric stew" (McCleskey, 2000) model of Nonner et al. (2000) assumes that the carboxylates of the four glutamates forming the selectivity EEEE locus move independently from each other and remove the requirement of other models that the ions pass through the selectivity filter in a single file. However, the model fails to explain specific contributions of the glutamates (Yang et al., 1993; Ellinor et al., 1995; Bahinski et al., 1997; Cloues et al., 2000) and the role of nonglutamate residues in permeation and selectivity (Yatani et al., 1994; Williamson and Sather, 1999; Feng et al., 2001; Cibulsky and Sather, 2003; Wang et al., 2005).

Allosteric models of Ca^{2+} channel permeation propose that the high-affinity selectivity filter undergoes Ca^{2+}-induced conformational changes produced by Ca^{2+} binding to a low-affinity site (Kostyuk et al., 1983; Lux et al., 1990; Mironov, 1992; Carbone et al., 1997). Although such allosteric models explain well all lines of evidence attributable to multi-ion pores, they involve assumptions about the voltage dependence of the on-off rates for the two sites that have not been tested yet. Akin to the view that the selectivity filter is allosterically regulated by Ca^{2+}, our recent findings (Babich et al., 2005) indicate that the apparent affinity of the pore in $Ca_V1.2$ channels to Ca^{2+} decreases as a part of voltage-dependent gating process upon activation.

Correspondence to Roman Shirokov: roman.shirokov@umdnj.edu

O. Babich's present address is Molecular Pharmacology Department, AstraZeneca R&D, Södertälje, Sweden.

Blocking polyvalent cations may also interact with channel gating. Obejero-Paz et al. (2004) found that in open channels, the on-rate for yttrium (Y^{3+}) block of T-type Ca^{2+} channels was increased in comparison to the closed state and suggested that this is because Ca^{2+} ions vacate the blocking site by passing through the open channel. Biagi and Enyeart (1990) found that Gd^{3+} not only reduces macroscopic current magnitude (tonic block) but also accelerates current decay during depolarization (use-dependent block). The acceleration of current decay was observed both in Ca^{2+} and in Ba^{2+}. Since Ca^{2+} and Ba^{2+} currents were presumed to inactivate by fundamentally different mechanisms, Biagi and Enyeart (1990) proposed that the use-dependent effect of Gd^{3+} occurs because it blocks open channels more potently than closed channels. Beedle et al. (2002) presented evidence that Y^{3+} ions accelerate inactivation of Ba^{2+} currents through $Ca_V1.2$ and $Ca_V2.1$ channels. They also found that they could manipulate kinetics of inactivation of Ba^{2+} currents without affecting the apparent affinity of Y^{3+} block of peak currents. The authors argued against a single-site mechanism for both processes and proposed that trivalent metal ions accelerate inactivation of Ba^{2+} currents through unblocked channels by binding to a site that is extracellular to the blocking site in the pore.

Here we suggest an alternate interpretation of these various findings. We investigate how blockade of L-type channels by Gd^{3+}, the blocker used to dissect ionic and gating currents in these channels, depends on voltage and concentration of permeant ions and characterize the competition between the blocker and permeant ions. Our results strongly support the view that the blocker causes both tonic and use-dependent effects at a single site; the tonic block is due to Gd^{3+} binding to closed channels, and the use-dependent effect reflects the reequilibration following an increase in the apparent on-rate for Gd^{3+} block. We propose that Gd^{3+} competes with permeant ions for an extracellular binding site at the mouth of the selectivity filter, and that the off-rate of the permeant ions increases during channel activation, leading to an increase in the on-rate for Gd^{3+} binding and a time-dependent decrease in current magnitude.

In the accompanying paper (Babich et al., 2007), we demonstrate that Gd^{3+} has little effect on voltage-dependent inactivation and dramatically reduces Ca^{2+}-dependent inactivation. Moreover, we present evidence that Gd^{3+} cannot occupy the blocking site in Ca^{2+}-inactivated channels. Therefore, our findings stimulate further structure function analysis of the link between selectivity and gating in Ca^{2+} channels.

MATERIALS AND METHODS

$Ca_V1.2$ channels were transiently expressed in tsA-201 cells as described previously (Ferreira et al., 1997). In all experiments except in some shown in Fig. 1, the pore-forming α_{1C} subunit was coexpressed together with β_{2a} and $\alpha_{2a}\delta$ subunit. Where it is noted in Fig. 1, the β_{2a} subunit was substituted by the β_3 subunit. The EEQE mutant of the third glutamate of the selectivity locus (the E1145Q substitution at the α_{1C} subunit) was done using the QuickChange XL kit from Stratagene and verified by sequencing. The CAM1234 mutant of calmodulin with aspartate to alanine mutations in all four EF hands (Putkey et al., 1989; Peterson et al., 1999) is a gift from G. Pitt (Columbia University, New York, NY).

The intracellular solution contained (in mM) 155 CsCl, 10 HEPES, 10 EGTA, 5 Mg-ATP. In most experiments, extracellular solutions contained (in mM) 150 NaCl, 10 Tris-Cl and 10 $BaCl_2$. Where it is noted, $SrCl_2$ or $CaCl_2$ was used instead of $BaCl_2$. In experiments shown in Fig. 8, the solutions with 2 and 20 mM $BaCl_2$ had 160 and 135 mM NaCl, respectively. 10 μM Gd^{3+} solutions were prepared daily from 1 mM $GdCl_3$ stock in water. Various lower concentrations of Gd^{3+} were done by sequential dilutions. Keeping Gd^{3+} solutions in polycarbonate, rather than in glass, tubes dramatically improved consistency of results at $[Gd^{3+}] < 1\mu M$. Every application of Gd^{3+} was followed by a wash in blocker-free solution to ensure reversibility of observed effects. All solutions were at pH 7.3, 310–320 mosmole/kg, and room temperature.

Ionic currents were recorded from cells with capacitance 10–20 pF and series resistance 3–10 MΩ, so that the membrane charging did not take longer than 150 μs. Up to 98% of the symmetric capacitive transient were routinely offset "on the fly" by the single time constant capacitance compensation circuitry of the Axopatch 200B amplifier (Molecular Devices). As we have shown before (Isaev et al., 2004; Babich et al., 2005), the combination of a relatively fast voltage clamp, high level of channel expression, and effective capacitance compensation allow us to record asymmetric transients of the $Ca_V1.2$ without acquiring control currents, which linearly depend on voltage, for further subtraction. Control pulses to adjust the circuitry were applied from the holding potential of −90 to −80 mV. If the RC settings change by >5% during the experiment, the experiment was discarded. For a 200-mV pulse spanning most of the useful voltage range, the residual linear transient corresponded to a transfer of <3 fC/pF of charge, while the saturating gating charge transfer from the expressed $Ca_V1.2$ channels was ∼30 fC/pF. Asymmetric currents were recorded at 1–2 kHz bandwidth and sampled at 10–50 kHz. Sets of pulses were applied at 0.01–0.03 Hz.

Measured values are presented as sample average ± SEM. Significance of difference of averages was established with the two-tailed *t* test (at the $P < 0.05$ level) using the normal distribution function and conventional estimates of standard deviation of the difference. Curve fitting was done by a nonlinear least-squares routine of SigmaPlot (SPSS Inc.). Fitted values are presented as estimate ± standard error of estimate (square root of the diagonal element in the covariance matrix).

Online Supplemental Material

The supplemental material (available at http://www.jgp.org/cgi/content/full/jgp.200709733/DC1) contains a kinetic scheme (Fig. S1) and associated steady-state calculations for a single-file mechanism involving competition between permeant and blocking cations for two sites in the permeation pathway.

RESULTS

Correlation between Tonic and Use-dependent Blocking Effects of Gd^{3+}

Experiments illustrated in Fig. 1 compared Gd^{3+} block of currents carried by different alkali-earth metal ions. The double-pulse protocols shown above the current traces were chosen to characterize block and availability

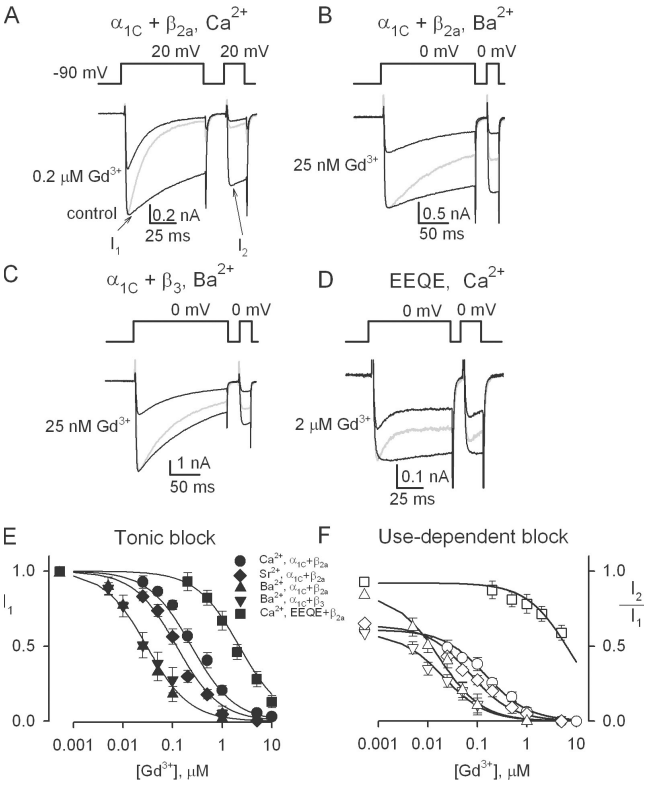

Figure 1. Tonic and use-dependent effects of Gd^{3+} in different conditions, in which blocker potency is altered. Gray lines illustrate traces elicited in the presence of blocker scaled to the magnitude of control currents in the absence of blocker. (A) In 10 mM Ca^{2+}, application of 0.2 μM Gd^{3+} reduced peak currents by about one half during the first pulse (I_1, tonic block), but to a much greater extent at the second pulse (I_2, use-dependent block). (B) With 10 mM Ba^{2+}, both tonic and use-dependent block occurred at 25 nM Gd^{3+}. (C) Although Ba^{2+} currents inactivated more rapidly in channels with the β_3 subunit rather than with the β_{2a} subunit (compare with B), tonic and use-dependent effects of Gd^{3+} were similar for both β subunits. (D) Exemplar Ca^{2+} currents through the EEQE mutant of the selectivity locus recorded with and without 2 μM Gd^{3+}. (E) Dose–response curves for tonic effect of Gd^{3+} determined for different experimental conditions (indicated). Tonic block is described by relative magnitude of peak current during the first pulse. Before averaging, each peak current measured in the presence of blocker was normalized to its value in the absence of blocker. n = 6–8 cells were analyzed for every experimental condition. Lines are best fits by hyperbolic equation $I = 1/(1 + [Gd^{3+}]/IC_{50})$, where IC_{50} is the concentration of half-block. For Ba^{2+} currents, $IC_{50} = 0.03 \pm 0.01$ μM. Only one fit is shown for cells with β_3 and β_{2a} subunits, because the IC_{50} was not significantly different in these cells. For Sr^{2+} currents, $IC_{50} = 0.12 \pm 0.02$ μM. For Ca^{2+} currents through the wild-type channel, $IC_{50} = 0.29 \pm 0.05$ μM. For Ca^{2+} currents trough the EEQE mutant in the selectivity locus, $IC_{50} = 2.1 \pm 0.4$ μM. (F) Dose–response curves for use-dependent blocking effects of Gd^{3+} determined for the same experimental conditions as in panel E. Use-dependent block is described by relative magnitude of peak current during the second pulse. Before averaging, the value of peak current at the second pulse was normalized to the value of peak current at the first pulse. Lines are best fits by hyperbolic equation $I = A/(1 + [Gd^{3+}]/IC_{50})$, where A is a constant and IC_{50} is the concentration of half-block. For Ba^{2+} currents in cells with the β_3 subunit, $A = 0.57 \pm 0.05$, $IC_{50} = 0.022 \pm 0.004$ μM. For Ba^{2+} currents in cells with the β_{2a} subunit, $A = 0.82 \pm 0.03$, $IC_{50} = 0.021 \pm 0.004$ μM. For Sr^{2+} currents, $A = 0.64 \pm 0.06$, $IC_{50} = 0.08 \pm 0.02$ μM. For Ca^{2+} currents trough the wild-type channel, $A = 0.61 \pm 0.05$, $IC_{50} = 0.15 \pm 0.03$ μM. For Ca^{2+} currents trough the EEQE mutant in the selectivity locus, $A = 0.92 \pm 0.07$, $IC_{50} = 7.1 \pm 2.6$ μM.

of maximal currents. Gray lines show the blocked current traces scaled to the peak of the unblocked current. Regardless of current carrier used, Gd^{3+} accelerated the post-peak decline in current, and currents at the second pulse were blocked to a greater extent than currents at the first pulse.

Fig. 1 E plots the extent of tonic block at different [Gd^{3+}]. It was determined by normalizing the peak current during the first pulse (I_1) to its value without Gd^{3+}. Use-dependent block is described by the ratio of peak currents I_2/I_1 and is shown in Fig. 1 F. In the absence of Gd^{3+}, the ratio characterizes availability of noninactivated channels after the first pulse. The decrease of the ratio with [Gd^{3+}] quantifies the additional reduction of current or the use-dependent block that occurs during the first pulse. The half-inhibition concentrations (IC_{50}) of Gd^{3+} for both tonic and use-dependent blocking effects followed the order $Ba^{2+} < Sr^{2+} < Ca^{2+}$.

Fig. 1 C illustrates experiments testing tonic and use-dependent block of Ba^{2+} currents through $Ca_V1.2$ channels with altered inactivation. Previously, Beedle et al. (2002) demonstrated that although inactivation of Ba^{2+} currents through $Ca_V2.1$ channels expressed together with the β_{2a} subunit was significantly slower than in channels with the β_1 subunit, the tonic block by Y^{3+} ions was not lessened. Furthermore, a mutation in the I–II linker region of the α_{1C} subunit of $Ca_V1.2$ reduced inactivation of Ba^{2+} currents but not the tonic block by Y^{3+}. With similar rationale, we analyzed how the blockage of $Ca_V1.2$ channels by Gd^{3+} ions is affected by a similar substitution of the β subunit. As expected (Olcese et al., 1994; Qin et al., 1996), Ba^{2+} currents through $Ca_V1.2$ channels expressed with the β_3 subunit inactivated much faster (compare traces in Fig. 1, B and C). Both tonic and use-dependent block of $Ca_V1.2$ channels with the β_3 subunit occurred at the same concentrations as with the β_{2a} subunit (up and down triangles in Fig. 1, E and F). These results are therefore similar to those reported by Beedle et al. (2002) for the effect of Y^{3+} ions on $Ca_V2.1$ channels with different β subunits.

A substantial increase in the IC_{50} for tonic block was observed for Ca^{2+} currents (0.29 ± 0.05 μM) compared with Ba^{2+} currents (0.03 ± 0.01 μM) (Fig. 1 E). Somewhat unexpectedly, the use-dependent block of Ca^{2+} currents also occurred at much higher concentrations of Gd^{3+} (Fig. 1 F). This result is compatible with the finding of Beedle et al. (2002) that both tonic block and acceleration of current decay by Y^{3+} ions in $Ca_V2.1$ channels are enhanced when [Ba^{2+}] is reduced from 20 to 2 mM.

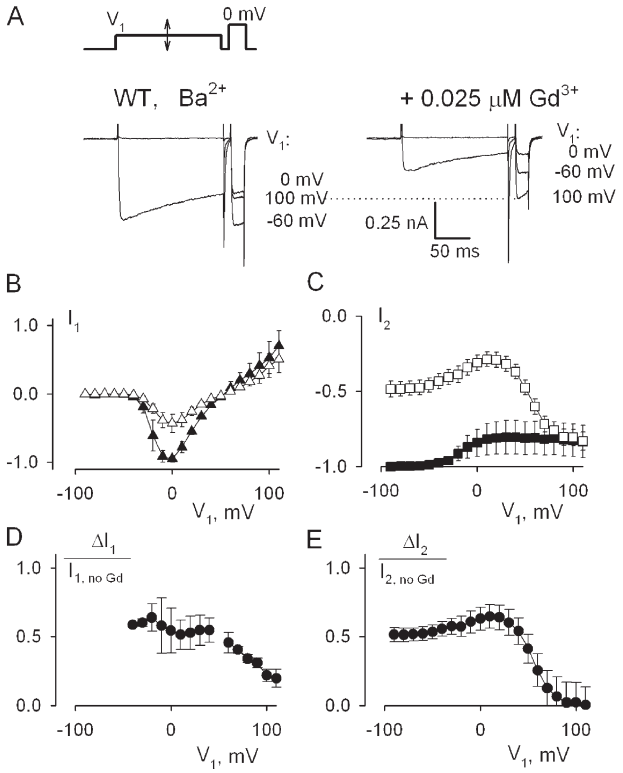

Figure 2. Voltage dependence of tonic and use-dependent block of Ba^{2+} currents as determined by the double-pulse experiments. Both components of Gd^{3+} block were relived at conditioning to large positive voltages. (A) Without Gd^{3+}, test Ba^{2+} current was less after conditioning at 0 mV in comparison with the −60-mV conditioning. Application of 25 nM Gd^{3+} increased the effect of conditioning at 0 mV. However, test currents in the presence of Gd^{3+} increased after conditioning to 100 mV to the levels that exceeded maximal blocked currents and reached the magnitude of unblocked test current after prepulse to 100 mV. Therefore, both use-dependent and tonic block were relieved by prepulse to 100 mV. (B) Peak current–voltage relationships for the first pulse. Filled symbols plot values in unblocked channels. Open symbols are for currents in the presence of Gd^{3+}. Before averaging ($n = 6$), in each cell peak currents at the first pulse were normalized to their maximal value in the absence of blocker. (C) Availabilities of current at the second pulse (test) plotted vs. voltage of the first pulse (conditioning). Before averaging, in each cell peak currents at the test pulse were normalized to their value determined with conditioning at −90 mV in the absence of blocker. Gd^{3+} did not significantly reduce Ba^{2+} currents measured after prepulses to voltages more positive than 70 mV. (D) Voltage dependence of tonic block determined from the data in B. (E) Voltage dependence of use-dependent block determined from the data in C.

Mutation of the third glutamate of the selectivity EEEE locus to glutamine (EEQE) is expected to reduce the apparent affinity of the tonic block by Gd^{3+} (Bahinski et al., 1997; Cloues et al., 2000). Fig. 1 D illustrates representative Ca^{2+} current traces for the EEQE mutant. Corresponding dependencies of tonic and use-dependent components of block on [Gd^{3+}] are plotted by squares in Fig. 1 (E and F). In the mutant, both tonic block and enhancement of current decay during depolarization required 10-fold higher concentration of Gd^{3+} in comparison with the wild-type channel.

Strikingly, Gd^{3+} enhances current decay and produces block of peak currents to a similar extent, in spite of the fact that the Gd^{3+} concentrations involved for Ba^{2+} and Ca^{2+} currents in the wild-type and Ca^{2+} currents in the mutant differ by an order of magnitude. This suggests that Gd^{3+} competition for the same site is involved in both block and current decay. The observed correlation between IC_{50}s for tonic and use-dependent effects strongly implicates Gd^{3+} binding to the selectivity filter as the cause of both components of block.

Voltage Dependence of Gd^{3+} Block

If both tonic and use-dependent components of Gd^{3+} block are due to Gd^{3+} binding in the pore, they should be relieved at high positive voltages by the Woodhull effect, i.e., electrodiffusion of charged blocker into the blocking site at the permeation pathway depends on the transmembrane potential (Woodhull, 1973). We assessed the voltage dependence of the block using double-pulse voltage protocols similar to those in Fig. 1, except that the first pulse was applied to various voltages. Fig. 2 A illustrates exemplar tracings of Ba^{2+} currents for first pulse voltages to −60, 20, and 100 mV. Here and in some other figures below, the outward currents during conditioning pulses to large positive voltages are out of scale, and so are not shown.

Corresponding peak current–voltage relationships for first pulse voltages from −90 to 120 mV are shown in Fig. 2 B. Before averaging, peak currents were scaled to their values measured in the absence of Gd^{3+} at 0 mV. Extent of tonic block was quantified as the relative reduction of peak current during the first pulse upon application of Gd^{3+} (Fig. 2 D). Similar to other studies of trivalent metal ions (Beedle et al., 2002), tonic block by Gd^{3+} was more efficient for inward rather than outward currents. Peak currents at the second pulse are plotted in Fig. 2 C versus voltage at the first pulse. Before averaging, the values in each cell were scaled to the magnitude of current at the second pulse recorded in the absence of Gd^{3+} and with the first pulse to −100 mV. Without blocker, peak current during the second pulse reflects availability of noninactivated channels after the first pulse. With blocker, it reflects availability of unblocked noninactivated channels. Relative reduction of current during the second pulse characterizes the sum of tonic and use-dependent block. It is plotted versus voltage of the first pulse in Fig. 2 E.

Gd^{3+} block of Ba^{2+} currents in the second pulse was maximal when the first pulse was near 0 mV. The blockage of currents during the second pulse was relieved when the first pulse went to high positive voltages. In fact, Ba^{2+} current measured after prepulse to 100 mV was practically unaffected by 0.025 μM Gd^{3+}, which would cause ∼50% block without the prepulse. The relief of

channel blockade by strong positive pulses had been observed previously for various types of Ca^{2+} channels and inorganic blockers (Lux et al., 1990; Thevenod and Jones, 1992), indicating that positive voltages retard or prevent entry of blocking cations into the pore. Because the rate of Gd^{3+} block is likely to be diffusion limited (see the data shown below), it cannot be $>10^9\ M^{-1}s^{-1} \times 25\ 10^{-9}\ M = 25\ s^{-1}$. Therefore, the brief (10 ms) interpulse at −90 mV in experiments shown in Fig. 2 was not long enough for Gd^{3+} ions to reenter and block Ba^{2+} currents at the second pulse. Simultaneous relief of tonic and use-dependent block of Ba^{2+} currents strongly indicates that Gd^{3+} causes both effects by binding inside the permeation pathway.

Because of pronounced current-dependent inactivation, the availability of Ca^{2+} current at the second pulse has "U-shaped" voltage dependence even in the absence of Gd^{3+}. Therefore, we compared the voltage dependencies of Gd^{3+} blockage of Ca^{2+} currents in the wild-type channels (Fig. 3) and in mutants with reduced Ca^{2+}-dependent inactivation (Figs. 4 and 5). The voltage pulse protocol was similar to that in Fig. 2. Fig. 3 B shows the availability of Ca^{2+} current in the second pulse as a function of voltage of the first pulse (similar to that in Fig. 2 C). As expected, Ca^{2+} currents through the wild-type channels in the absence of Gd^{3+} (circles in Fig. 3 A) inactivated the most after the first pulse to 10 mV. Addition of Gd^{3+} had several effects on the voltage dependence of the availability of Ca^{2+} currents. At negative voltages (less than −40 mV), the currents were reduced due to the tonic blocking effect. At voltages where channels activate (from −40 to 30 mV), Gd^{3+} further decreased the availability of current due to the use-dependent effect. At voltages more positive than 30 mV, the block was relieved similar to what was observed for Ba^{2+} currents (Fig. 2). Although at 0.1 μM of Gd^{3+} the block was completely relieved after the first pulse to 150 mV, ∼20% of current remained blocked at 1 μM of Gd^{3+}. While the onset of the use-dependent block occurred at about the same voltages (from −40 to 30 mV), the relief of block required stronger depolarization for greater amounts of the blocker.

The enhancement of block at voltages corresponding to activation of channels indicates that the activation/inactivation gating mechanism was rate limiting for the current decay in this voltage range. The reduction of current decay observed at positive voltages is a "classical" feature of an effect of transmembrane voltage on ion movement through the channel. This suggests that a reduced influx of Gd^{3+}, or charge carrier, or both, into the channel probably underlies the relief of block at these voltages. The contributions of Gd^{3+} and charge carrier influx are discussed separately below, but both mechanisms may be involved.

First, it is possible that the acceleration of current decay in the presence of Gd^{3+} merely represents the slow

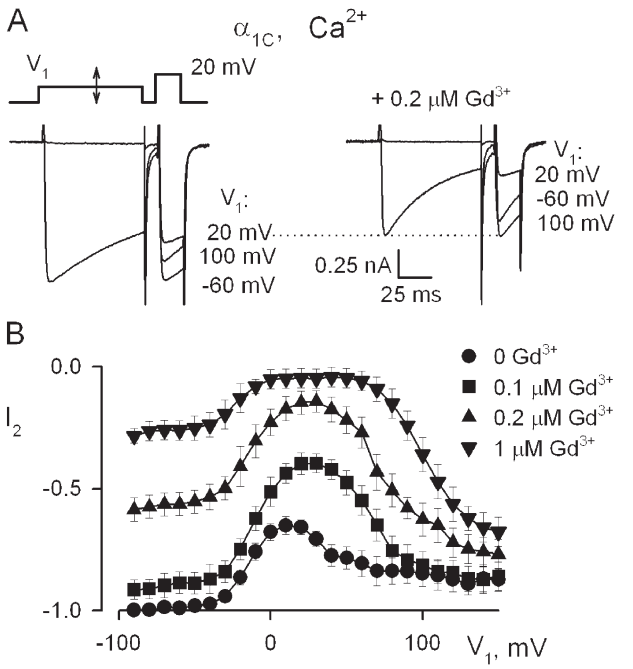

Figure 3. At any concentration of Gd^{3+}, Ca^{2+} currents through the wild-type channel were minimal after conditioning at intermediate voltages. (A) Without Gd^{3+}, test Ca^{2+} current was less after conditioning at 20 mV in comparison with the −60-mV conditioning. Application of 0.2 μM Gd^{3+} increased the effect of conditioning at 20 mV. However, the additional reduction of test current due to Gd^{3+} was partially relieved by conditioning at 100 mV. (B) Availabilities of test Ca^{2+} current plotted vs. conditioning voltage. Before averaging (n = 8), in each cell peak currents at the test pulse were normalized to their value determined with conditioning at −90 mV in the absence of blocker. In the absence of Gd^{3+} (circles), test currents were minimal after prepulses to 10 mV due to Ca^{2+}-dependent inactivation. 0.1 μM Gd^{3+} (squares) enhanced the reduction of currents at intermediate voltages, but it did not significantly reduce Ca^{2+} currents measured after prepulses to voltages more positive than 90 mV. At greater amounts of Gd^{3+} (indicated), the voltage-dependent relief of block required stronger prepulses and it was not complete.

diffusion of Gd^{3+} into the binding site. The diffusion-limited binding of the blocker to a site in the permeation pathway might explain both the U-shaped voltage dependence of current decay and the difference in kinetics in Ca^{2+} and Ba^{2+}. Since block of Ca^{2+} current required greater [Gd^{3+}], Gd^{3+} influx into the blocking site is greater in Ca^{2+} and it would take stronger positive voltage steps to reduce the block to the same extent as for Ba^{2+} currents. The increase in the apparent affinity of the channel for Gd^{3+} block that is observed as the use-dependent effect could be because of channel activation/opening, inactivation, or both. The second possibility is that Ba^{2+} flux itself contributes to Ba^{2+} current inactivation (Ferreira et al., 1997). In this case, both inactivation and additional block by Gd^{3+} are reduced at positive voltages because Ba^{2+} flux is reduced. This would be consistent with the idea of Beedle et al. (2002)

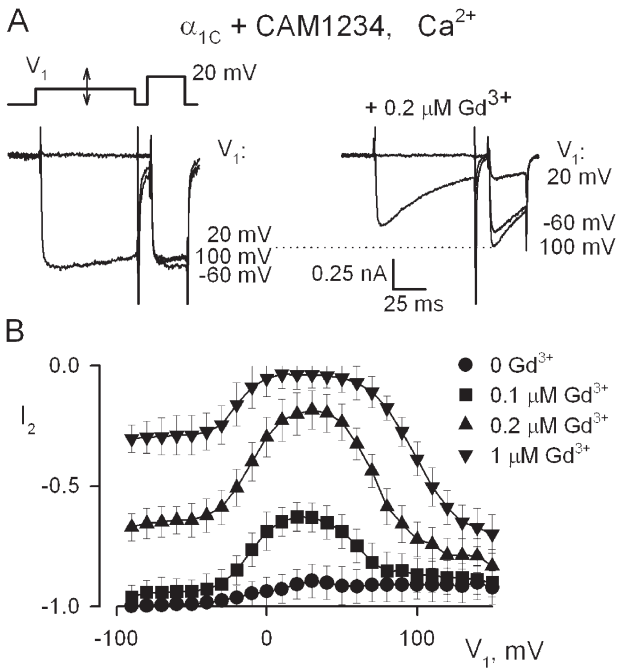

Figure 4. Gd^{3+} block of Ca^{2+} currents through the channels with Ca^{2+}-dependent inactivation diminished by coexpression with the mutant apo-calmodulin CAM1234. (A) Without Gd^{3+}, conditioning to 20 mV had little effect on test Ca^{2+} current. At 0.2 μM Gd^{3+}, conditioning at 20 mV caused significant reduction of Ca^{2+} current even though Ca^{2+}-dependent inactivation was small. The reduction of test current due to Gd^{3+} was partially relieved by conditioning at 100 mV. (B) Availabilities of test Ca^{2+} current plotted vs. conditioning voltage. Before averaging ($n = 5$), in each cell peak currents at the test pulse were normalized to their value determined with conditioning at −90 mV in the absence of blocker. In the absence of Gd^{3+} (circles), the availability of test current was nearly a sigmoid function of voltage. With Gd^{3+}, test currents were minimal after prepulses to intermediate voltages despite Ca^{2+}-dependent inactivation was absent. With 0.1 μM Gd^{3+} (squares), the magnitude of Ca^{2+} currents measured after prepulses to voltages more positive than 80 mV was the same as without Gd^{3+}. At greater amounts of Gd^{3+} (indicated), the voltage-dependent relief required stronger prepulses and it was not complete.

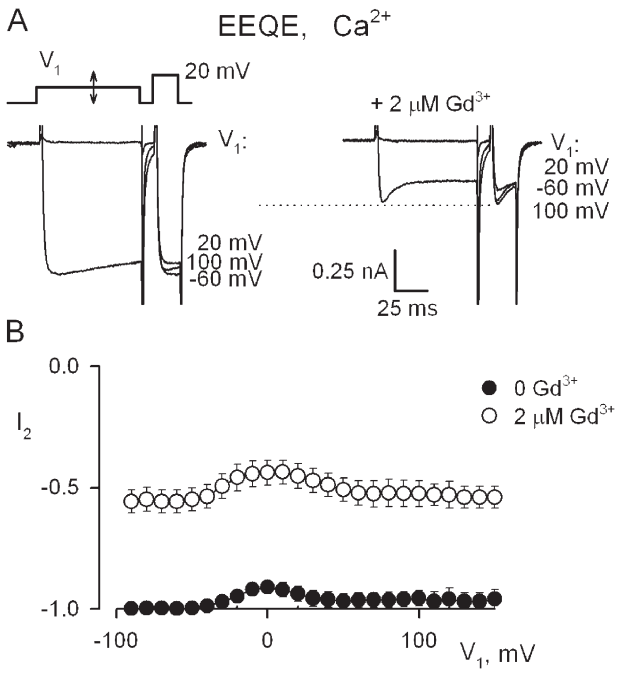

Figure 5. Gd^{3+} block of Ca^{2+} currents through the EEQE mutant of the selectivity locus. The mutant diminishes Ca^{2+}-dependent inactivation (Zong et al., 1994) and Gd^{3+} block (Fig. 1). (A) Without Gd^{3+}, conditioning prepulses to different voltages (indicated) had little effect on test Ca^{2+} current. Addition of 2 μM Gd^{3+} blocked test currents by about one half regardless of the voltage of conditioning pulse (indicated). (B) Availabilities of test Ca^{2+} current plotted vs. conditioning voltage. Before averaging ($n = 5$), in each cell peak currents at the test pulse were normalized to their value determined with conditioning at −90 mV in the absence of blocker. In the absence of Gd^{3+} (filled circles), the availability of test current was nearly independent on voltage showing dramatic reduction of inactivation in the EEQE mutant. With 2 μM Gd^{3+} (open circles), the extent of additional block at intermediate voltages was small and there was no relief of block even at 150 mV.

that Gd^{3+} accelerates inactivation of Ba^{2+} currents. However, the findings below establish that the use-dependent effect of Gd^{3+} does not require the channel to undergo current-dependent inactivation.

Use-dependent Block and Ca^{2+}-dependent Inactivation

The use-dependent effect is likely to occur because Gd^{3+} binding is linked to activation gating. It could be a direct link to preopening transitions, or because of ionic current in open channel (Obejero-Paz et al., 2004), or because of inactivation (Beedle et al., 2002). To determine whether Ca^{2+}-dependent inactivation plays a role, we studied the voltage dependence of Gd^{3+} block in channels that had their Ca^{2+}-dependent inactivation impaired by the mutant apo-calmodulin CAM1234 (Peterson et al., 1999). The exemplar traces are shown in Fig. 4 A and the availability of current in the second pulse is plotted in Fig. 4 B. In these cells, the extent of inactivation is small (Fig. 4 B, circles). However, the effect of Gd^{3+} was very similar to that in channels with normal calmodulin (Fig. 3). Therefore, control of inactivation by Ca^{2+}/calmodulin is not involved in the acceleration of Gd^{3+} block.

Another possibility to alter Ca^{2+}-dependent inactivation is the EEQE mutation of the selectivity locus (Zong et al., 1994). This mutation reduces ~10-fold the potency of Gd^{3+} to block the channels (Fig. 1). Fig. 5 illustrates the voltage dependence of availability of current in the EEQE mutant in the absence of Gd^{3+} and with 2 μM of Gd^{3+} that caused nearly half-block. In the mutant, there was little use-dependent block and almost no relief from the block after prepulses to positive voltages. This is in contrast to the wild-type channel, where the block was nearly completely relieved at high voltages. In Discussion, we reason that the voltage dependence of

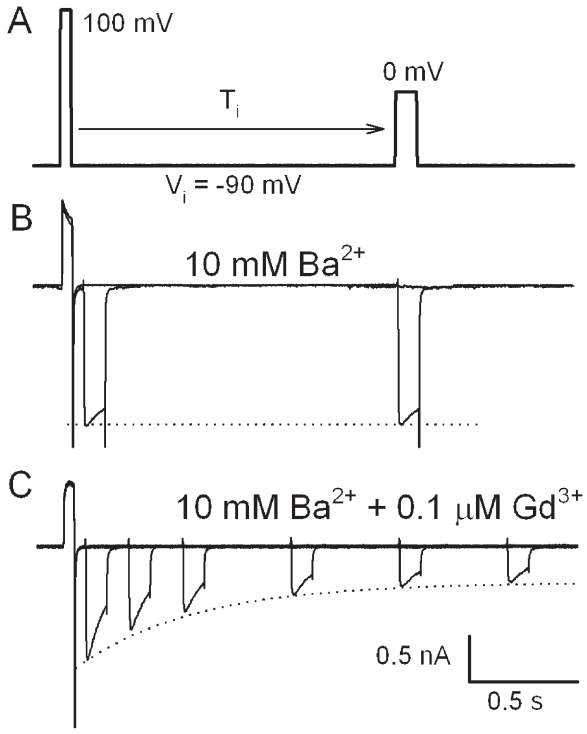

Figure 6. Reblock of closed channels. (A) Double-pulse protocol used to study kinetics of block of closed channels during interpulses of various duration (T_i) and voltage (V_i). (B) Prepulses to 100 mV had no measurable effect on test Ba^{2+} currents in the absence of Gd^{3+}. (C) In presence of Gd^{3+}, the magnitude of test current recorded briefly after the prepulse was similar to that without Gd^{3+}. Test currents decreased with increasing interpulse duration. After long interpulses, test currents became equal to those without prepulse (tonic block).

block at a site in the permeation pathway should vary with the $[Gd^{3+}]/K_D$ ratio (K_D is the dissociation constant at 0 mV). Since the extent of block was similar in the mutant and in the wild type, the voltage dependence of block should be similar despite very different concentrations of Gd^{3+}. The absence of relief of Gd^{3+} block in Fig. 5 indicates that the mechanism of the block is different in the mutant and probably involves binding of Gd^{3+} to a different site that might also be responsible for the voltage-independent component of block in the wild type at high (>1 μM) Gd^{3+} concentrations (e.g., in Fig. 3).

Kinetics of Gd^{3+} Block of Closed Channels

We studied the kinetics of block of Ba^{2+} currents with double-pulse protocols similar to those illustrated in Fig. 6 A. The first pulse to positive voltage relieved the block, and kinetics of Gd^{3+} rebinding were monitored by changes of current at the second (test) pulse applied after an interpulse of various duration and voltage. In the absence of the blocker, the prepulse significantly changed neither the magnitude nor kinetics of test current (Fig. 6 B). This is consistent with that the voltage-dependent facilitation (Sculptoreanu et al., 1993) of cardiac L-type channels expressed with the β_{2a} subunit is small (Cens et al., 1996).

In the presence of blocker (Fig. 6 C), the prepulse caused long-lasting elevation of the test current similar to that described for T-type channels blocked by Y^{3+} (Obejero-Paz et al., 2004). The onset of reduction of test currents reflects the kinetics of reblock during the interpulse. Therefore we investigated how the kinetics are affected by voltage and permeant ions (Figs. 7 and 8).

To avoid possible problems due to current run-down and other long-term instability, pairs of traces were obtained as shown in Fig. 7 A. First, a test pulse from −90 mV elicited a control current without a prepulse. The control currents are shown by gray lines in Fig. 7 (B and C). After holding the cell at −90 mV for 30 s, the test current was acquired. The prepulse to 100 mV and an interpulse of duration T_i and voltage V_i preceded the test pulse. Fig. 7 B illustrates the tracings obtained without Gd^{3+} and with V_i = −60 mV and T_i indicated. Test currents were reduced slightly after prolonged conditioning at −60 mV, apparently due to inactivation. With 25 nM Gd^{3+} in the bathing solution (Fig. 7 C), the control current was less due to tonic block, and the prepulse caused significant increase of test currents elicited shortly after the prepulse. After longer interpulse periods, test currents continued to decrease, reflecting faster and more potent blockage at the −60-mV interpulse.

Averaged amplitudes of test currents obtained after interpulses of different duration and voltage are plotted in Fig. 7 D. Before averaging, the amplitude of the test current was normalized to that of the control current of the pair of traces obtained by the protocols described in Fig. 7 A. Thus, the relative magnitude of test currents obtained after long interpulses at −90 mV is 1. The lines in Fig. 7 D are best fits by the sum of two exponentials and a constant. The relative weight of the rapid exponential (~2 s^{-1}) increased with the interpulse voltage from ~40% at −90 mV to ~65% at −45 mV. At the same time, the relative weight of the slow exponential (<0.5 s^{-1}) changed from 0 at −90 mV to ~30% at −45 mV. Therefore, the two kinetic components were well separated. Since the rapid component reflects reblock at −90 mV, it is likely to describe the kinetics in noninactivated channels at more positive voltages. The slow component is likely to be due to voltage-dependent inactivation that occurred during the interpulse.

From the rate (k) and the relative contribution (E) of the rapid component we determined the rates of block ($k^+ = k_{on}[Gd^{3+}]$) and the off-rate (k_{off}) using the pseudo-first order approximation: $k^+ = kE/(1 + E)$ and $k^- = k/(1 + E)$. They are plotted in Fig. 7 E as functions of voltage. Importantly, the rate of binding steeply increased at voltages more positive than −60 mV. At the same time, the rate of unbinding was much less dependent on voltage.

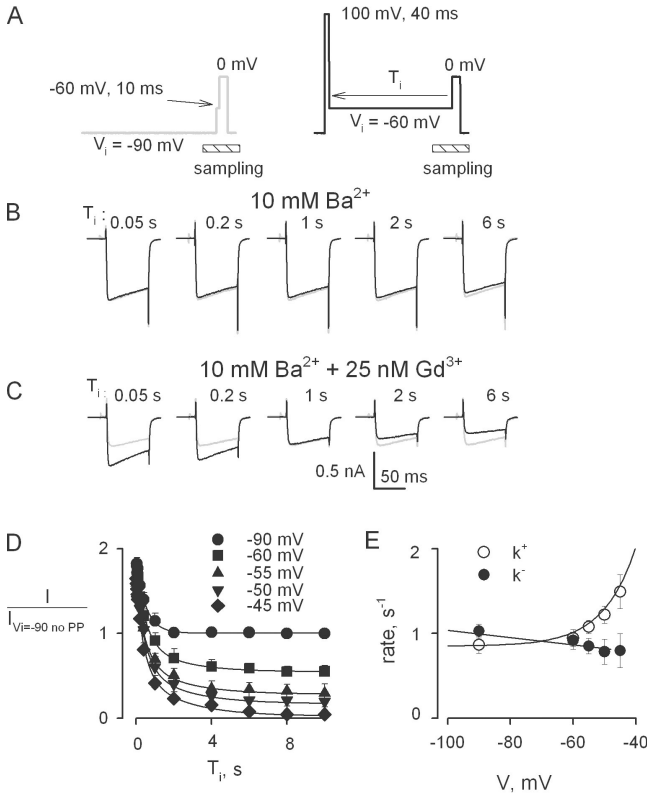

Figure 7. Dependence of block of closed channels on voltage. (A) Test currents were determined by pairs. First, a control current was recorded without prepulse (gray line). After 30 s at the holding potential of −90 mV, the pulse protocol shown by black line was applied. To avoid heavy-duty cycle effect, the next pair of currents was determined after holding the cell at −90 mV for at least 30 s. (B) Pairs of control (gray lines) and test Ba^{2+} currents (black lines) elicited without Gd^{3+} as described in A for the interpulse voltage of −60 mV and different interpulse duration (indicated). Test currents after 6 s interpulse were reduced by <10% because of inactivation at −60 mV. (C) Pairs of control and test Ba^{2+} currents elicited in the presence of 25 nM Gd^{3+} for the interpulse voltage of −60 mV. Control currents were reduced due to tonic block at the holding potential of −90 mV. Test currents recorded with a 50-ms interpulse were nearly as large as currents in the absence of Gd^{3+}, but they decreased with the duration of the interpulse and became smaller than the control currents for interpulses longer than 2 s. (D) Averaged magnitudes of test currents determined at different interpulse voltage. n = 6–10 for each [Ba^{2+}]. The lines are best fits by the sum of two exponential and a constant: $I = ae^{-bt} + ce^{-dt} + e$. For −90 mV interpulse, a = 0.84 ± 0.12, b = 1.89 ± 0.07 s^{-1}, c = 0, e = 1. For −60 mV, a = 0.86 ± 0.10, b = 1.91 ± 0.06 s^{-1}, c = 0.35 ± 0.12, d = 0.46 ± 0.08 s^{-1}, e = 0.55 ± 0.08. For −55 mV, a = 0.85 ± 0.09, b = 1.93 ± 0.07 s^{-1}, c = 0.39 ± 0.10, d = 0.43 ± 0.08 s^{-1}, e = 0.28 ± 0.07. For −50 mV, a = 0.95 ± 0.12, b = 2.01 ± 0.07 s^{-1}, c = 0.44 ± 0.10, d = 0.43 ± 0.09 s^{-1}, e = 0.17 ± 0.07. For −45 mV, a = 1.01 ± 0.11, b = 2.29 ± 0.08 s^{-1}, c = 0.51 ± 0.12, d = 0.44 ± 0.08 s^{-1}, e = 0.03 ± 0.03. (E) Estimates of rates of reblock determined from the fast kinetic component of reduction of test currents defined in D. $k^- = b/(1 + E)$, $k^+ = bE/(1 + E)$, where b is the rate of the fast component and $E = a/(a + c + e)$. The lines are drawn by eye.

Using a similar approach, we investigated how the rates of Gd^{3+} block depend on Ba^{2+} concentration (Fig. 8). The interpulse voltage was −90 mV, so there was no interference of inactivation (Fig. 8 A). As described above, 25 nM Gd^{3+} under these conditions caused nearly half-block when [Ba^{2+}] was 10 mM. However, >80% of the current was blocked by addition of the same amount of Gd^{3+} to the bathing solution with 2 mM Ba^{2+} (Fig. 8 B). The extent of blockage did not decrease as much when [Ba^{2+}] was changed from 10 to 20 mM. The kinetics of reblock were the slowest at 20 mM and the fastest at 2 mM Ba^{2+}. Fig. 8 C shows the averaged magnitude of test current determined in a manner similar to that in Fig. 7 D. The corresponding rates of block are shown in Fig. 8 D. Similar to the effect of voltage (Fig. 7 E), the rate of block, but not the off-rate, changed with the concentration of Ba^{2+}.

The on-rate for Gd^{3+} block can be obtained simply from $k_{on} = k^+ / [Gd^{3+}]$. From the data in Figs. 7 and 8, the on-rate was 3.5 ± 0.5 10^7 $M^{-1}s^{-1}$ at −90 mV in 10 mM Ba^{2+} solution. In 10 mM Ca^{2+}, the on-rate was estimated for the −90-mV interpulse and 0.2 μM Gd^{3+} in experiments similar to those in Figs. 7 and 8 (not depicted). It was 1.4 ± 0.6 10^7 $M^{-1}s^{-1}$. Therefore both in Ca^{2+} and in Ba^{2+}, Gd^{3+} binding at −90 mV was limited by processes other than its diffusion.

The observations in Figs. 7 and 8 indicate that the blocker competes with the charge carrier for a binding site within the voltage-sensitive portion of the permeation pathway. Since the rates of block, but not the off-rates, were affected by voltage and charge carrier concentration, we conclude that the accessibility of this site to the blocker is limited by the rate of evacuation of the charge carrier from the site. Importantly, the interpulse voltages used in these experiments did not cause channel opening and so evacuation of the charge carrier could not have occurred through open channels as proposed by Obejero-Paz et al. (2004) for the Y^{3+} blockage of T-type channels. Instead, the acceleration of block with increasing voltage appears to be linked to the charge movement that precedes the opening step. This is illustrated by the experiment described below.

For the experiment shown in Fig. 9, the pulse protocol involved a 40-ms-long prepulse to 200 mV to relieve Gd^{3+} block; for the control currents (in gray), the 200-mV prepulse was omitted. Then, the voltage was stepped to −200 mV for 40 ms to ensure full closure of channels before an interpulse to various voltages and a test pulse to 20 mV are applied. Currents in 10 mM Ca^{2+} and 1 μM Gd^{3+} are compared in Fig. 9 B for various interpulse voltages. After −100 mV interpulse voltage, the test current at 0 mV increased after prepulse to 200 mV because the 100-ms interpulse was too brief for complete reblock (the rate of reblock is $\sim 10^{-6}$ M × 1.4 10^7 $M^{-1}s^{-1} = 14\ s^{-1}$), as shown in Fig. 9 B by the difference between traces *b* and *a* elicited with and without the

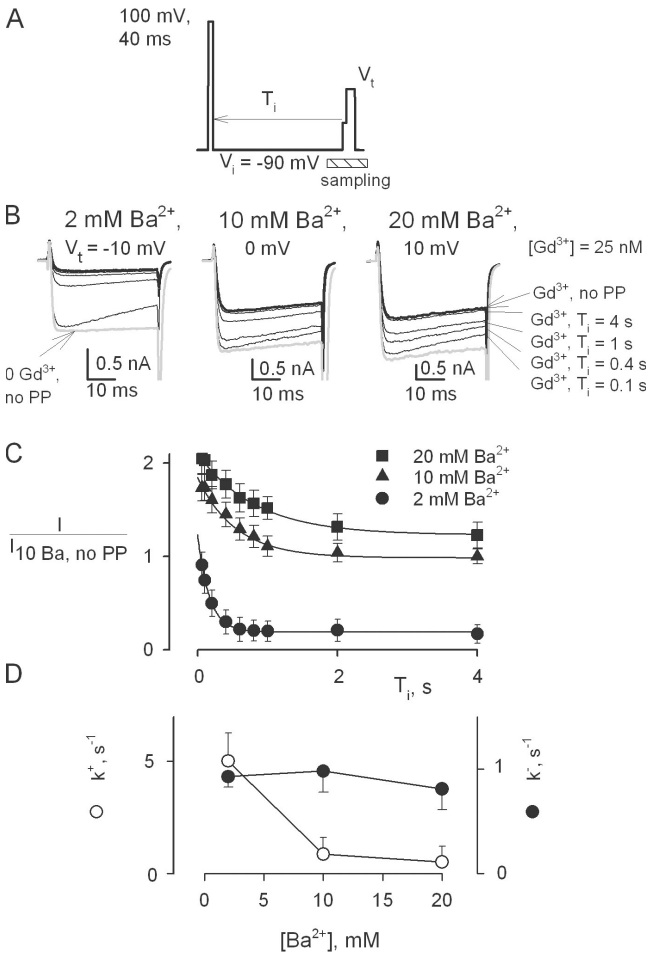

Figure 8. Dependence of block of closed channels on [Ba^{2+}]. (A) Voltage pulse protocol to study kinetics of reblock at –90 mV. (B) Test currents obtained with interpulses of different duration (indicated). Thick lines show test currents obtained without prepulses. Gray lines show test currents without Gd^{3+} and black lines are traces obtained in the presence of 25 nM Gd^{3+}. (C) Averaged magnitudes of test currents determined for different [Ba^{2+}] (indicated). n = 5–8 for each [Ba^{2+}]. The lines are best fits by the sum of an exponential and a constant: $I = ae^{-bt} + c$. For 2 mM, a = 1.04 ± 0.07, b = 5.94 ± 0.13 s^{-1}, c = 0.19 ± 0.06. For 10 mM, a = 0.86 ± 0.13, b = 1.83 ± 0.08 s^{-1}, c = 1. For 20 mM, a = 0.88 ± 0.12, b = 1.21 ± 0.07 s^{-1}, c = 1.23 ± 0.13. (D) Estimates of rates of reblock determined from the reduction of test currents defined in A. $k^- = b/(1 + E)$, $k^+ = bE/(1 + E)$, where b is the rate of reduction of current and $E = a/(a + c)$.

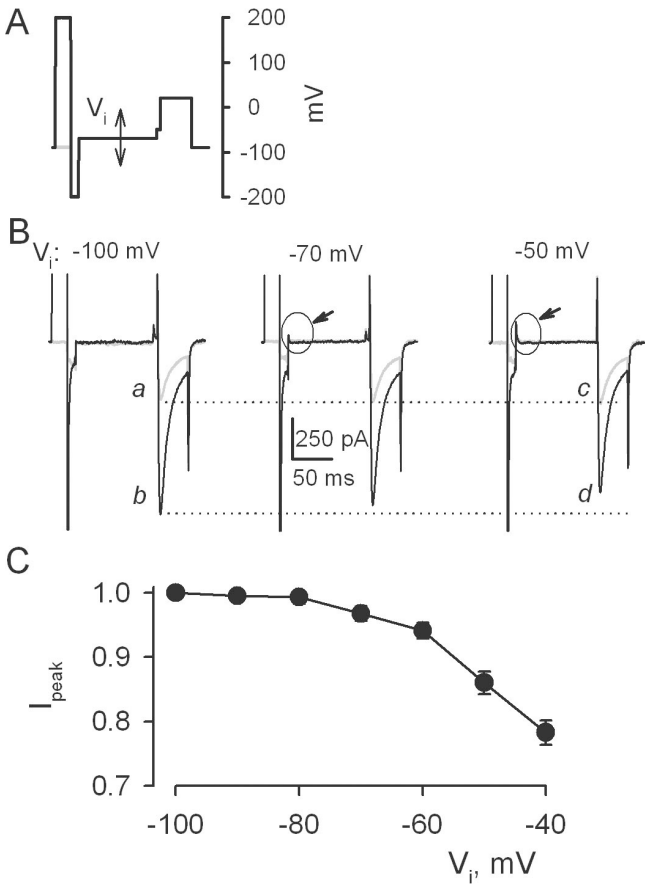

Figure 9. Acceleration of Gd^{3+} block occurs at voltage steps that do not cause ionic currents. (A) Voltage pulse protocol. (B) Exemplar Ca^{2+} currents recorded in the presence of 1 μM Gd^{3+} with (black lines) and without (gray lines) the prepulse to 200 mV. Control currents (traces *a* and *c*) did not depend on the interpulse voltage V_i (indicated), but test currents recorded after the prepulse (traces *b* and *d*) decreased with V_i in the range where no ionic currents could be recorded (e.g., at −70 mV). At the same time, the voltage steps from −200 mV to V_i caused significant gating currents (indicated by arrows). (C) Averaged magnitude of test currents vs. voltage of the interpulse. Before averaging, each value was normalized to the magnitude at V_i = −100 mV determined in the same cell (n = 4).

unblocking prepulse to 200 mV. When the interpulse voltage was more positive than −70 mV, the difference between traces with (*d*) and without (*c*) the unblocking prepulse was less than between *b* and *a* (Fig. 9 C). Therefore, significantly more channels were reblocked during the −50 mV interpulse in comparison with the −100 mV interpulse. The observed increase of the rate of reblock confirms that the access of Gd^{3+} to the blocking site increases during depolarization that does not open the channel. The increased accessibility correlates with preopening gating currents (Fig. 9 B, circled segment). These findings directly link the increase of the on-rate for Gd^{3+} block to the preopening voltage-dependent transitions in the channel.

Kinetics of Gd^{3+} Block of Open Channels

The kinetics of Gd^{3+} block that develops during voltage pulses activating ionic currents were studied using a 40-ms-long prepulse to 200 mV to relieve Gd^{3+} block. Then, the voltage was stepped to −200 mV for 40 ms to ensure full closure of channels before test pulses are applied (Fig. 10 A). Fig. 10 (B and C) shows examples of Ba^{2+} and Ca^{2+} currents elicited in the absence of Gd^{3+} by such pulse protocols. The prepulse had little effect in the absence of Gd^{3+}.

In presence of Gd^{3+}, prepulses to 200 mV increased the magnitude of currents during test pulses, allowing

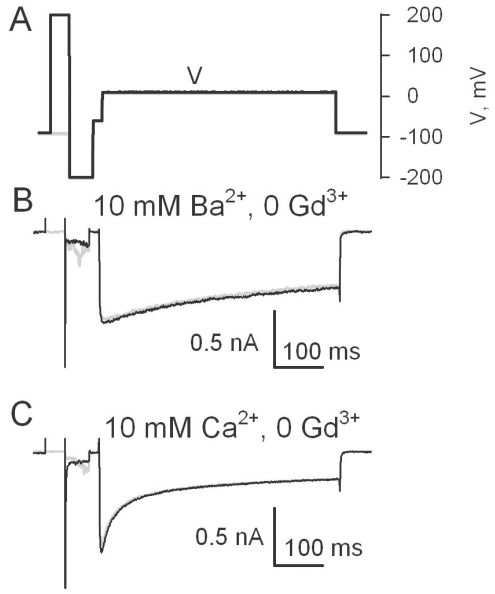

Figure 10. Prepulses used to study reblock of open channels changed neither magnitude nor kinetics of test currents in the absence of Gd^{3+}. Exemplar currents recorded with (black lines) and without (gray lines) the prepulse to 200 mV. (A) Double-pulse protocol used to study kinetics of block of open channels during voltage steps (V) that activate ionic currents. (B) Prepulses to 200 mV had no measurable effect on test Ba^{2+} currents in the absence of Gd^{3+}. The currents were recoded at V = 0 mV. (C) Prepulses to 200 mV had no measurable effect on test Ca^{2+} currents in the absence of Gd^{3+}. The currents were recoded at V = 20 mV in a different cell.

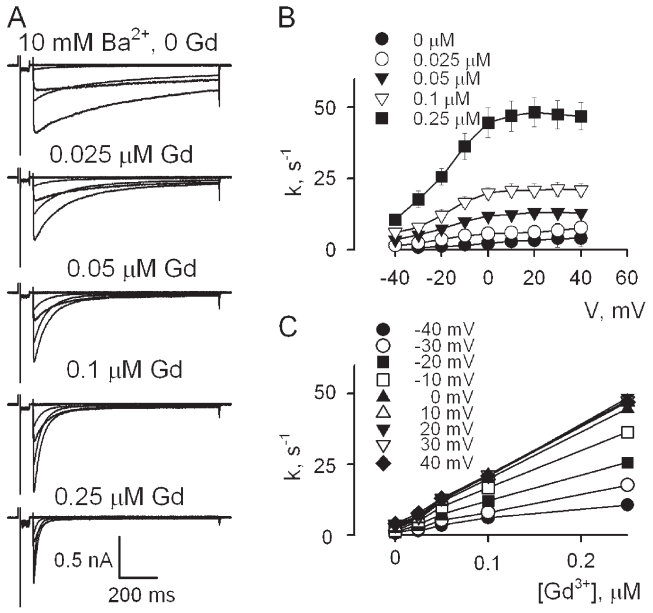

Figure 11. Kinetics of block of Ba^{2+} currents. (A) Test Ba^{2+} currents elicited by a pulse protocol similar to that in Fig. 10. Traces are shown for test voltages to −60–40 mV, increment 20 mV. Because of the prepulse to 200 mV, tonic block by Gd^{3+} was removed and reduction of currents during test voltage steps reflected reblock of open channels. (B) The averaged rates of best fits by the sum of an exponential and a constant to the decay phase of test currents recorded as in A are plotted vs. test voltage for different $[Gd^{3+}]$ (indicated). $n = 5$. (C) The averaged rates of current decay are plotted vs. $[Gd^{3+}]$ for different test voltages (indicated). The data are the same as in B.

us to analyze voltage dependence of blocking kinetics after activation of ionic currents. Fig. 11 illustrates the experiments with Ba^{2+} as the charge carrier. Exemplar traces are shown in Fig. 11 A for different concentrations of Gd^{3+}. Without Gd^{3+}, current decay was due to inactivation only and its rate was no greater than 0.4 s^{-1}. With Gd^{3+}, currents decayed more rapidly at every test voltage. The decay phases were fit by the sum of single exponential plus a constant. The averaged rates of the fits are plotted against voltage in Fig. 11 B. The lines connect the sets of points obtained at the concentration of Gd^{3+} indicated. At every concentration of Gd^{3+}, the voltage dependence of Gd^{3+} block was a sigmoid function of voltage, suggesting that the block was linked to activation gating either directly or via inactivation. The same data are plotted against concentration of Gd^{3+} in Fig. 11 C. The lines in this panel connect the sets of points obtained at the voltage indicated. The rates depended on concentration nearly linearly. At every voltage, the zero concentration intercepts of the linear regressions through the points at any voltage were not significantly different from zero. In the one-step pseudo-first order approximation of Gd^{3+} binding, the intercepts would be equal to the off-rate. Thus, the rate of current decay was nearly limited by Gd^{3+} entry into the blocking site. The maximal steepness of the rate vs. concentration plots in Fig. 11 C was achieved at voltages greater than −10 mV. It corresponds to the on-rate of $\sim 2 \times 10^8$ $M^{-1}s^{-1}$.

In Ca^{2+}, inactivation is much faster than in Ba^{2+}. Its significant contribution to kinetics of current decay distorted the determination of the rate of Gd^{3+} blockage (Fig. 12). However, at voltages more positive than 20 mV, inactivation was relatively small and the rate of current decay linearly depended on concentration Gd^{3+} (Fig. 12 C) with small zero concentration intercepts similar to that observed in experiments with Ba^{2+} (Fig. 11). Also, the rate of Ca^{2+} current decay was a sigmoid, not U-shaped, function of voltage at Gd^{3+} concentrations >0.5 μM. In 10 mM Ca^{2+}, the rate vs. concentration plots (Fig. 12 C) were the steepest at voltages >20 mV. The corresponding on-rate for Gd^{3+} block was $\sim 1 \times 10^8$ $M^{-1}s^{-1}$, which is half of that in 10 mM Ba^{2+}.

Link of Gd^{3+} to Voltage-dependent Activation Steps Preceding the Opening Step

Kinetics of Ca^{2+}/Ba^{2+} current decay in the presence of Gd^{3+} could be described simply as a sum of inactivation and Gd^{3+} block that is linked to activation gating. Such direct link explains well the enhancement of block with voltage. The simplest kinetic scheme that describes

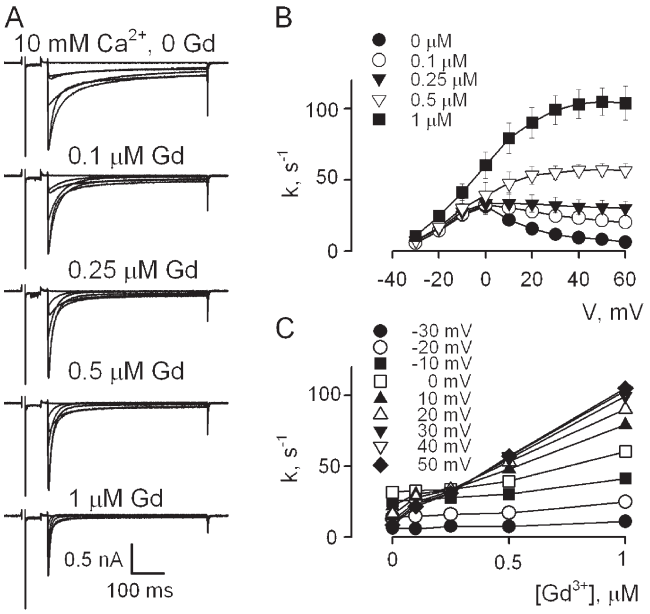

Figure 12. Kinetics of block of Ca^{2+} currents. (A) Test Ca^{2+} currents elicited similarly to that in Fig. 11. (B) The averaged rates of best fits by the sum of an exponential and a constant to the decay phase of test currents recorded as in A are plotted vs. test voltage for different $[Gd^{3+}]$ (indicated). $n = 4$. (C) The averaged rates of current decay are plotted vs. $[Gd^{3+}]$ for different test voltages (indicated). The data are the same as in B.

more potent binding of Gd^{3+} to open/activated channels is:

$$C \rightleftharpoons A \overset{Gd}{\rightleftharpoons} AGd$$

If, like in our experimental conditions, the activation step C↔A is more rapid than the block step and the rate of unbinding is slow, then the rate of current decay is limited by the availability of open/activated channels: $k = k_{on}[Gd^{3+}]k_V^+/(k_V^+ + k_V^-)$, where k_{on} is the on-rate of Gd^{3+} block, and k_V^+ and k_V^- are the voltage-dependent rates of the activation step. The factor $k_V^+/(k_V^+ + k_V^-)$ is analogous to the activation function of the Hodgkin-Huxley formalism. Indeed, the sigmoid dependence of the rate of Gd^{3+} block on voltage, as observed in experiments shown in Figs. 11 and 12, was very similar to that of activation of these channels.

Results of experiments that investigated Gd^{3+} block of "closed" channels (at voltages more negative than −45 mV) demonstrated that the rate of binding increased sharply at voltages −60 to −45 mV where the preopening transitions occur (Fig. 7 E). At the same time, the rate of Gd^{3+} binding increases with voltage over the range where the channels open (Fig. 11 B). The on-rates of Gd^{3+} block of closed (Fig. 7 E) and open (Fig. 11 B) channels are plotted together in Fig. 13 as a function of voltage. In both groups of experiments, the on-rates were determined at 10 mM Ba^{2+}. The data points

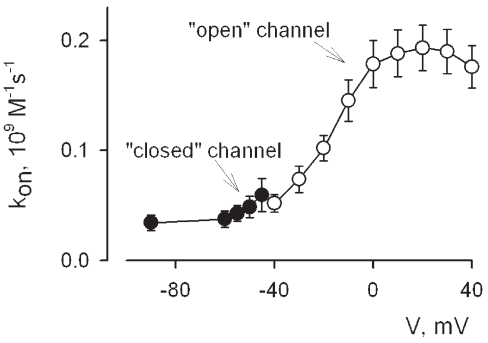

Figure 13. The on-rates of Gd^{3+} block of "closed" channels (filled symbols) and "open" channels (open symbols) fall on a single sigmoid that parallels the voltage dependence of the gating charge movement.

for open channels were taken from the dataset with 0.1 mM Gd^{3+} (squares in Fig. 11 B), which was distorted by inactivation the least. Both datasets appear to fall on a single sigmoid and we therefore suggest that there is no fundamental difference in the block of closed and open channels. The declining phase observed at positive voltages is due to the Woodhull effect.

Gd^{3+} Block and Gating Currents

Since Gd^{3+} binds to closed and activated/open channels and the channels can activate (move gating charge) when Gd^{3+} is bound, a minimal kinetic scheme that describes Gd^{3+} binding is that of state-dependent binding:

$$\begin{array}{ccc} Gd\,C & \rightleftharpoons & A\,Gd \\ \downarrow\uparrow & & \downarrow\uparrow \\ CGd & \rightleftharpoons & AGd \end{array}$$

In this case, a more potent binding to activated/open (A) in comparison with resting/closed (C) channels would require that the equilibrium in the CGd↔AGd step is shifted toward the AGd state. It follows that blocked channels should activate (move gating charge) at more negative voltages in comparison with the unblocked channels. The following experiment demonstrates that this was not the case.

Addition of Gd^{3+} (5–20 μM) to 10 mM Ca^{2+} extracellular solution had been used previously to block ionic currents and thus isolate gating currents in these channels. Gating currents in Ca^{2+} and other voltage-gated channels start to occur at voltages somewhat more negative than those at which any ionic currents through the channels could be recorded. In the experiments shown in Fig. 14, the asymmetric currents (i.e., compensated for the capacitive transients that linearly depend on voltage) were recorded at voltages below −20 mV. In 10 mM Ca^{2+}, measurable ionic inward currents could be observed at voltages more positive than −40 mV. Below −40 mV, ionic currents did not contaminate traces of the asymmetric capacitive transients. None of the transients were

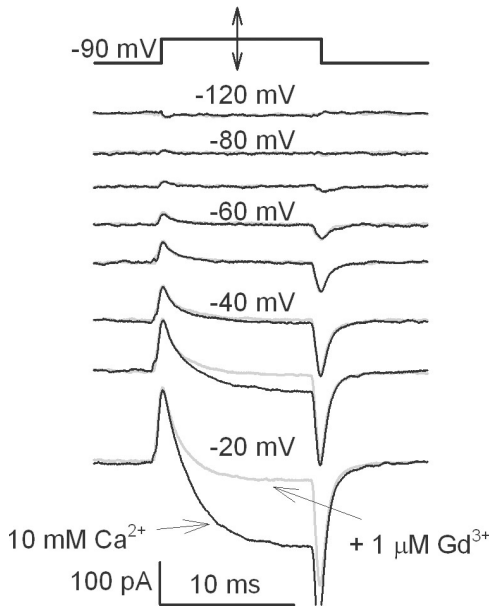

Figure 14. Gd^{3+} block does not change gating currents recorded at voltages before channel opening. Black traces, asymmetric currents (the sum of ionic and gating currents) in the bathing solution with 10 mM Ca^{2+}; gray traces, asymmetric currents in the bathing solution with 10 mM Ca^{2+} and 1 μM Gd^{3+}.

altered by addition of 1 μM Gd^{3+}. We did similar experiments on a large number (>100) of cells during previous studies of gating currents in these channels and never observed an increase of gating current transient that would indicate a negative shift of their voltage dependence. Instead, we observed some decrease/slowing of gating currents at $[Gd^{3+}]$ >20 μM.

DISCUSSION

Voltage-dependent Increase in the On-rate for Gd^{3+} Binding Explains both Tonic and Use-dependent Effects

Results presented in this paper allow us to explain the complex voltage dependence of block by Gd^{3+} (Figs. 2 and 3) by a combination of two mechanisms that change the apparent affinity of the single binding site located in the permeation pathway: (1) the changes in the accessibility of the pore that are linked to activation gating, as Biagi and Enyeart (1990) suggested, and (2) the direct influence of voltage on movement of Gd^{3+} into/from the binding site (Woodhull, 1973).

The possibility that Gd^{3+} block is enhanced at voltages where channels activate because of a link to current-dependent inactivation appears to be unlikely because the potency of Gd^{3+} for the use-dependent block of Ca^{2+} currents was not altered by the CAM1234 mutation (Figs. 3 and 4). In the accompanying paper (Babich et al., 2007), we demonstrate that Gd^{3+} block does not enhance inactivation of either Ca^{2+} or Ba^{2+} currents. Such enhancement is expected if Gd^{3+} binds more potently to inactivated channels. Therefore, the use-dependent effect of Gd^{3+} requires neither current- nor voltage-dependent inactivation.

The shift of the relief phase of current availability to more positive voltages with increasing concentration of Gd^{3+} (Fig. 3) is consistent with the Woodhull effect. Due to the Woodhull effect, the apparent dissociation constant for the blocker is: $K_{D,eff} = K_D e^{(\delta z|e^-|V/k_BT)}$, where K_D is the dissociation constant at 0 mV, δ is the portion of the electric field that drops at the binding site, $k_BT/z|e^-| \approx 8$ mV. The relatively low steepness of the voltage dependence of relief ($k_BT/\delta z|e^-| > 25$ mV) is consistent with the view that the blocking site is at the extracellular edge of permeation pathway ($\delta < 0.3$). The voltage of half restoration of current could be derived assuming that the proportion of unblocked channels is $1/(1 + [Gd^{3+}]/K_{D,eff})$. Then, $V_{1/2} = (k_BT/\delta z|e^-|) \times \ln([Gd^{3+}]/K_D)$. For the 10-fold change of $[Gd^{3+}]$ from 0.1 to 1 μM, the observed shift of the voltage of half restoration was ≈60 mV, which is in good agreement with the following calculation: $60 \text{ mV} \approx 25 \text{ mV} \times \ln(10) \approx 25 \text{ mV} \times 2.3$.

Not all of the block of Ca^{2+} currents could be relieved by pulses to 200 mV when $[Gd^{3+}]$ was >0.1 μM (Figs. 3–5) This was unlikely to be due to a more rapid reblock of closed channels during the 10-ms interpulse interval, as the rate of reblock was $<14\ s^{-1}$. It is possible that Gd^{3+} at concentrations >0.1 μM binds to a second site of lower affinity. The second site could be either in, or outside, of the permeation pathway. If the pore is occupied by two Gd^{3+} ions, the Woodhull effect should be lessened because the ions would screen out the transmembrane field between them.

Regardless of the exact mechanism of the link between Gd^{3+} block and activation, the observed correlation between the potencies of Gd^{3+} for tonic and use-dependent effects (Fig. 1) and the relief of both components of block at high positive voltages strongly indicates that the two components occur at the same site in the permeation pathway.

Gd^{3+} Competes with Permeating Ions for Site that Has Low Affinity for Permeating Ions

Since Gd^{3+} block at voltages below the activation range is clearly not limited by diffusion, the off-rate for the competing permeant ions can be estimated. A simple one-site scheme,

$$\mathbf{AM} \underset{}{\overset{M^{2+}}{\rightleftharpoons}} \mathbf{A} \overset{Gd^{3+}}{\rightleftharpoons} \mathbf{AGd}$$

gives the lower estimate of the evacuation rate of the competing ion M^{2+} from the Gd^{3+} binding site, because additional binding steps would only delay the exchange. In the single-site mechanism, the apparent dissociation constant for Gd^{3+} block is: $K_{D,eff} = K_{D,Gd}(1 + [M^{2+}]/K_{D,M})$, where $K_{D,Gd}$ and $K_{D,M}$ are the "true" dissociation constants.

Assuming that the "true" on-rates for Gd^{3+} and competing ion are similar (e.g., limited only by diffusion), the effective on-rate for Gd^{3+} binding is $k_{on,eff} = k_{off,M}/(K_{D,M} + [M^{2+}])$. If the site is nearly saturated with respect to the competing ion, then $k_{on,eff} \approx k_{off,M}/[M^{2+}]$. Thus, the measured on-rates of tonic Gd^{3+} block in 10 mM Ba^{2+} ($3.5 \times 10^7\ M^{-1}s^{-1}$) or Ca^{2+} ($1.4 \times 10^7\ M^{-1}s^{-1}$) correspond to the off-rates $3.5 \times 10^5\ s^{-1}$ (Ba^{2+}) and $1.4 \times 10^5\ s^{-1}$ (Ca^{2+}). Therefore, $K_{D,M}$ is in the order of 10^{-4}–10^{-3} M at voltages below the activation range. The competition described above explains well why Gd^{3+} that blocks in the submicromolar range is affected by changes in concentration of permeant ions in the millimolar range.

During activation, the on-rate for Gd^{3+} block increases ~10-fold (Fig. 13) to become nearly diffusion limited. At the same time, the extent of block also increases (Figs. 2 and 3). To satisfy the competition mechanism discussed above, the off-rate for competing permeant ions, but not for Gd^{3+}, should increase at least as much.

An interesting analogy that allows us to propose a mechanism of how this could be achieved at molecular level comes from the structure–function studies of the competition between lanthanides and Ca^{2+} to the EF-hand Ca^{2+}-binding motifs. Some EF hands contain asparagine residue in the third Ca^{2+} coordinating position. Substitution of an acidic aspartate for the native asparagine in a model EF-hand decreases the optimal divalent affinity at least 380-fold and increases the optimal trivalent affinity 16-fold, yielding an overall 6,000-fold shift toward trivalent selectivity (Drake et al., 1997). Since such behavior is not observed for any neutral side chain substitutions, the substitution specifically alters the stability of the metal-occupied state: it enhances the stability of the trivalent cation–occupied site and destabilizes the divalent cation–occupied site. The effect of substitution was explained by the electrostatic repulsion model, according to which the excess negative charge density triggered by the substitution of too many acidic side chains into the coordinating array will require additional positive charge to stabilize the occupied site.

Similarly, we suggest that activation gating destabilizes the binding site at the entrance to the selectivity filter where the permeant/blocking ions shed off their water shell. The destabilization (for example, by an addition of negative charge density) would affect the off-rate of permeant ions to a much greater extent in comparison with that of blocking ions.

Regardless of the exact mechanism of how activation gating affects the competition between Gd^{3+} and permeant ions, the relatively high apparent on-rate for Gd^{3+} block determined in conditions when it is not limited by diffusion (−90 mV, 10 mM Ba^{2+}, Fig. 7) strongly suggests that the affinity of the site to permeant ions is in 0.1–1 mM range in closed channels. The affinity decreases at least 10-fold upon activation. This suggests that the site may determine the dependence of current amplitude on the concentration of the divalent charge carrier ($K_D \approx 10$ mM).

The view that the blocking site has relatively low affinity for permeant ions appears to contradict to the strong effect of the EEQE mutation (Figs. 1 and 5). Point mutants of the third glutamate in the selectivity EEEE locus have the greatest impact among the four on the affinity for Ca^{2+} and Co^{2+} to block currents carried by monovalent ions (for review see Sather and McCleskey, 2003). The glutamates of the second and the third repeat have been suggested to contribute to the deeper high affinity binding site of the two-site mechanism involving ion–ion interaction (Yang et al., 1993). However, if the third glutamate instead contributes to the low affinity entry site of the stair-step mechanism (Dang and McCleskey, 1998), it could be as important for determining the occupancy of the high-affinity site by Ca^{2+}. The two-site competition scheme can explain the observed reduction of both tonic and use-dependent components of Gd^{3+} block in the EEQE mutant by assuming that the affinities of the entry site for Gd^{3+} and Ca^{2+} are reduced. It also explains the reduced efficacy of submicromolar Ca concentrations in blocking Na^+ currents in the EEQE mutant. To get into the high affinity site of the multi-ion pore, extracellular Ca^{2+} would need to pass first through the low-affinity entry site. If, in the EEQE mutant, the affinity of the entry site for Ca^{2+} is too low, Na^+ or other monovalent ions will occupy it most of the time, thus blocking Ca^{2+} from the central site. Corresponding calculations of the redistribution of competing ions are shown in Fig. S1 (available at http://www.jgp.org/cgi/content/full/jgp.200709733/DC1) for Ca^{2+} block of Na^+ currents, tonic and use-dependent block by Gd^{3+}, and for the proposed effects of the EEQE mutant via changes in the low-affinity entry site.

Gd^{3+} Block Is Linked to the Preopening Transitions, but Not to Gating Currents

The findings of experiments in Figs. 7 and 9 indicate that the increased potency of Gd^{3+} to block is linked to the preopening voltage-dependent transitions in the channel. These transitions are thought to follow the movement of the voltage-sensing portions of the channel measured as gating current. Since Gd^{3+} binding stabilizes the state of the channel with its voltage sensor(s) in the trans/active position, the equilibrium between the cis/resting and trans/active positions of the sensor should be shifted toward the trans position when Gd^{3+} is present. Somewhat unexpectedly, however, Gd^{3+} did not change the preopening gating currents (Fig. 14). Several possibilities can account for this observation. First, the measured gating currents in L-type Ca^{2+} channels are too large to be caused by the S4 movement (the principal source of gating currents in other voltage-dependent channels) in those channels that open to pass ionic currents (Kostyuk et al., 1981; Bean, Rios, 1989;

Isaev et al., 2004). In this case, the effect of Gd^{3+} on gating currents might go undetected because of a large contribution from channels that open the gate at the cytosolic mouth but are not capable, for some reason, of lowering the affinity of the extracellular entry for Ca^{2+}. Another possibility could be that the rearrangement of the extracellular entry is not linked to the movement of S4 segments, but it gains its voltage dependency from another independent sensor that contributes little to the measured gating currents. Charged residues in the pore structure itself could participate in such a mechanism, as shown in recent experiments and theoretical works on the KcsA channel by Berneche and Roux (2005), Blunck et al. (2006), and Cordero-Morales et al. (2006a,b).

Conclusion

Our results show that both tonic and use-dependent block of L-type Ca currents by Gd^{3+} result from the interaction of Gd^{3+} with a single site in an extracellular portion of the permeation pathway. The site is accessible to Gd^{3+} in closed channels and also binds permeant ions with a low affinity. Use-dependent block reflects an increase in the on-rate of Gd^{3+} that is linked to channel activation and involves conformational changes that further decrease the affinity of the site for competing permeant ions. A two-site single file stair step model for entry of Ca^{2+} into the selectivity filter accurately simulates tonic and use-dependent block, as well as the blockade of monovalent currents by Ca^{2+} in mutant and wild-type channels. Although the exact location of this site is unknown, we suggest that it might represent the entrance to the permeation pathway where ion dehydration occurs.

The authors are grateful to Andy Harris for valuable suggestions and discussions.

The work was supported by National Institutes of Health grants MH62838 to R. Shirokov, and HL49932 to J. Reeves.

Olaf S. Andersen served as editor.

Submitted: 3 January 2007
Accepted: 20 April 2007

REFERENCES

Almers, W., and E.W. McCleskey. 1984. Non-selective conductance in calcium channels of frog muscle: calcium selectivity in a single-file pore. *J. Physiol.* 353:585–608.

Armstrong, C.M., and J. Neyton. 1991. Ion permeation through calcium channels. A one site model. *Ann. NY Acad. Sci.* 635:18–25.

Babich O., D. Isaev, and R. Shirokov. 2005. Role of extracellular Ca^{2+} in gating of $Ca_V1.2$ channels. *J. Physiol.* 565:709–715.

Babich, O., V. Matveev, A.L. Harris, and R. Shirokov. 2007. Ca^{2+}-dependent inactivation of $Ca_V1.2$ channels prevents Gd^{3+} block: does Ca^{2+} block the pore of inactivated channels? *J. Gen. Physiol.* 129:477–483.

Bahinski, A., A. Yatani, G. Mikala, S. Tang, S. Yamamoto, and A. Schwartz. 1997. Charged amino acids near the pore entrance influence ion-conduction of a human L-type cardiac calcium channel. *Mol. Cell. Biochem.* 166:125–134.

Berneche, S., and B. Roux. 2005. A gate in the selectivity filter of potassium channels. *Structure.* 13:591–600.

Bean, B.P., and E. Rios. 1989. Nonlinear charge movement in mammalian cardiac ventricular cells. Components from Na and Ca channel gating. *J. Gen. Physiol.* 94:65–93 (published erratum appears in *J. Gen. Physiol.* 94:401)

Beedle, A.M., J. Hamid, and G.W. Zamponi. 2002. Inhibition of transiently expressed low- and high-voltage-activated calcium channels by trivalent metal cations. *J. Membr. Biol.* 187:225–238.

Biagi, B.A., and J.J. Enyeart. 1990. Gadolinium blocks low- and high-threshold calcium currents in pituitary cells. *Am. J. Physiol.* 259: C515–C520.

Blunck, R., J.F. Cordero-Morales, L.G. Cuello, E. Perozo, and F. Bezanilla. 2006. Detection of the opening of the bundle crossing in KcsA with fluorescence lifetime spectroscopy reveals the existence of two gates for ion conduction. *J. Gen. Physiol.* 128:569–581.

Carbone, E., H.D. Lux, V. Carabelli, G. Aicardi, and H. Zucker. 1997. Ca^{2+} and Na^{+} permeability of high-threshold Ca^{2+} channels and their voltage-dependent block by Mg^{2+} ions in chick sensory neurones. *J. Physiol.* 504:1–15.

Cens, T., M. Mangoni, S. Richard, J. Nargeot, and P. Charnet. 1996. Coexpression of the β2 subunit does not induce voltage-dependent facilitation of the class C L-type Ca channel. *Pflugers Arch.* 431:771–774.

Cibulsky, S.M., and W.A. Sather. 2003. Control of ion conduction in L-type Ca^{2+} channels by the concerted action of S5-6 regions. *Biophys. J.* 84:1709–1719.

Cloues, R.K., S.M. Cibulsky, and W.A. Sather. 2000. Ion interactions in the high-affinity binding locus of a voltage-gated Ca^{2+} channel. *J. Gen. Physiol.* 116:569–586.

Cordero-Morales, J.F., L.G. Cuello, Y. Zhao, V. Jogini, D.M. Cortes, B. Roux, and E. Perozo. 2006a. Molecular determinants of gating at the potassium-channel selectivity filter. *Nat. Struct. Mol. Biol.* 13:311–318.

Cordero-Morales, J.F., L.G. Cuello, and E. Perozo. 2006b. Voltage-dependent gating at the KcsA selectivity filter. *Nat. Struct. Mol. Biol.* 13:319–322.

Dang, T.X., and E.W. McCleskey. 1998. Ion channel selectivity through stepwise changes in binding affinity. *J. Gen. Physiol.* 111:185–193.

Drake, S.K., M.A. Zimmer, C. Kundrot, and J.J. Falke. 1997. Molecular tuning of an EF-hand-like calcium binding loop. Contributions of the coordinating side chain at loop position 3. *J. Gen. Physiol.* 110:173–184.

Ellinor, P.T., J. Yang, W.A. Sather, J.F. Zhang, and R.W. Tsien. 1995. Ca^{2+} channel selectivity at a single locus for high-affinity Ca^{2+} interactions. *Neuron.* 15:1121–1132.

Feng, Z.P., J. Hamid, C. Doering, S.E. Jarvis, G.M. Bosey, E. Bourinet, T.P. Snutch, and G.W. Zamponi. 2001. Amino acid residues outside of the pore region contribute to N-type calcium channel permeation. *J. Biol. Chem.* 276:5726–5730.

Ferreira, G., J. Yi, E. Rios, and R. Shirokov. 1997. Ion-dependent inactivation of barium current through L-type calcium channels. *J. Gen. Physiol.* 109:449–461.

Hess, P., and R.W. Tsien. 1984. Mechanism of ion permeation through calcium channels. *Nature.* 309:453–456.

Isaev, D., K. Solt, O. Gurtovaya, J.P. Reeves, and R. Shirokov. 2004. Modulation of the voltage sensor of L-type Ca^{2+} channels by intracellular Ca^{2+}. *J. Gen. Physiol.* 123:555–571.

K ostyuk, P.G., O.A. Krishtal, and V.I. Pidoplichko. 1981. Calcium inward current and related charge movements in the membrane of snail neurones. *J. Physiol.* 310:403–421.

Kostyuk, P.G., S.L. Mironov, and Y.M. Shuba. 1983. Two ion-selective filters in the calcium channel of the somatic membrane of mollusk neurons. *Neirofiziologiia.* 15:420–427.

Kuo, C.C., and P. Hess. 1993a. Ion permeation through the L-type Ca^{2+} channel in rat phaeochromocytoma cells: two sets of ion binding sites in the pore. *J. Physiol.* 466:629–655.

Kuo, C.C., and P. Hess. 1993b. Characterization of the high-affinity Ca binding sites in the L-type Ca channel pore in rat phaeochromocytoma cells. *J. Physiol.* 466:657–682.

Lux, H.D., E. Carbone, and H. Zucker. 1990. Na^+ currents through low-voltage-activated Ca^{2+} channels of chick sensory neurones: block by external Ca^{2+} and Ca^{2+}. *J. Physiol.* 430:159–188.

McCleskey, E.W. 2000. Ion channel selectivity using an electric stew. *Biophys. J.* 79:1691–1692.

Mironov, S.L. 1992. Conformational model for ion permeation in membrane channels: a comparison with multi-ion models and applications to calcium channel permeability. *Biophys. J.* 63:485–496.

Nonner, W., L. Catacuzzeno, and B. Eisenberg. 2000. Binding and selectivity in L-type calcium channels: a mean spherical approximation. *Biophys. J.* 79:1976–1992.

Obejero-Paz, C.A., I.P. Gray, and S.W. Jones. 2004. Y^{3+} block demonstrates an intracellular activation gate for the α1G T-type Ca^{2+} channel. *J. Gen. Physiol.* 124:631–640.

Olcese, R., N. Qin, T. Schneider, A. Neely, X. Wei, E. Stefani, and L. Birnbaumer. 1994. The amino terminus of a calcium channel β subunit sets rates of channel inactivation independently of the subunit's effect on activation. *Neuron.* 13:1433–1438.

Peterson, B.Z., C.D. DeMaria, J.P. Adelman, and D.T. Yue. 1999. Calmodulin is the Ca^{2+} sensor for Ca^{2+}-dependent inactivation of L-type calcium channels. *Neuron.* 22:549–558.

Putkey, J.A., H.L. Sweeney, and S.T. Campbell. 1989. Site-directed mutation of the trigger calcium-binding sites in cardiac troponin C. *J. Biol. Chem.* 264:12370–12378.

Qin, N., R. Olcese, J. Zhou, O.A. Cabello, L. Birnbaumer, and E. Stefani. 1996. Identification of a second region of the β-subunit involved in regulation of calcium channel inactivation. *Am. J. Physiol.* 271:C1539–C1545.

Sather, W.A., and E.W. McCleskey. 2003. Permeation and selectivity of calcium channels. *Annu. Rev. Physiol.* 65:133–159.

Sculptoreanu, A., E. Rotman, M. Takahashi, T. Scheuer, and W.A. Catterall. 1993. Voltage-dependent potentiation of the activity of cardiac L-type calcium channel α1 subunits due to phosphorylation by cAMP-dependent protein kinase. *Proc. Natl. Acad. Sci. USA.* 90(21):10135–10139.

Thevenod, F., and S.W. Jones. 1992. Cadmium block of calcium current in frog sympathetic neurons. *Biophys. J.* 63:162–168.

Wang, X., T.A. Ponoran, R.L. Rasmusson, D.S. Ragsdale, and B.Z. Peterson. 2005. Amino acid substitutions in the pore of the $Ca_V1.2$ calcium channel reduce barium currents without affecting calcium currents. *Biophys. J.* 89:1731–1743.

Woodhull, A.M. 1973. Ionic blockage of sodium channels in nerve. *J. Gen. Physiol.* 61:687–708.

Williamson, A.V., and W.A. Sather. 1999. Nonglutamate pore residues in ion selection and conduction in voltage-gated Ca^{2+} channels. *Biophys. J.* 77:2575–2589.

Yang, J., P.T. Ellinor, W.A. Sather, J.F. Zhang, and R.W. Tsien. 1993. Molecular determinants of Ca^{2+} selectivity and ion permeation in L-type Ca^{2+} channels. *Nature.* 366:158–161.

Yatani, A., A. Bahinski, M. Wakamori, S. Tang, Y. Mori, T. Kobayashi, and A. Schwartz. 1994. Alteration of channel characteristics by exchange of pore-forming regions between two structurally related Ca^{2+} channels. *Mol. Cell. Biochem.* 140:93–102.

Zong, S., J. Zhou, and T. Tanabe. 1994. Molecular determinants of calcium-dependent inactivation in cardiac L-type calcium channels. *Biochem. Biophys. Res. Commun.* 201:1117–1123.